doi:10.1038/nature11981

SUPPLEMENTARY NOTES

Our validated model highlights at least 12 novel regulators that either positively or negatively impact the Th17 program (**Fig. 4** and **5**). Remarkably, we found that these and known regulators are organized in two tightly coupled, self reinforcing and mutually antagonistic modules, whose coordinated action may explain how the balance between Th17, Treg, and other effector T cells is maintained, and how progressive directional differentiation of Th17 cells is achieved while repressing differentiation of other T cell subsets. We further validated and characterized the function of four of the 12 regulators – Mina, Fas, Pou2af1, and Tsc22d3 – by undertaking Th17 differentiation of T cells from corresponding knockout mice or with ChIP-Seq binding profiles.

Other regulators also highlight exciting predictions. For example, among the novel 'Th17 positive' factors is the zinc finger E-box binding homeobox 1 Zeb1, which is early-induced and sustained in the Th17 time course (**Supplementary Fig. 13a**), analogous to the expression of many known key Th17 factors. Zeb1 knockdown decreases the expression of Th17 signature cytokines (including IL-17A, IL-17F, and IL-21) and TFs (including Rbpj, Maff, and Mina) and of late induced cytokine and cytokine receptor genes ($p<10^{-4}$, cluster *C19*, **Supplementary Tables 5** and **7**). It is bound in Th17 cells by ROR-γt, Batf and Stat3, and is down-regulated in cells from Stat3 knockout mice (**Supplementary Fig. 13a**). Interestingly, Zeb1 is known to interact with the chromatin factor Smarca4/Brg1 to repress the E-cadherin promoter in epithelial cells and induce an epithelial-mesenchymal transition[1]. Smarca4 is a regulator in all three network models (**Fig. 2d**) and a member of the 'positive module' (**Fig. 4b**). Although it is not

differentially expressed in the Th17 time course, it is bound by Batf, Irf4 and Stat3 (positive regulators of Th17), but also by Gata3 and Stat5 (positive regulators of other lineages, **Supplementary Fig. 13a**). Chromatin remodeling complexes that contain Smarca4 are known to displace nucleosomes and remodel chromatin at the IFN-γ promoter and promote its expression in Th1 cells[2]. There are also potential Smarca4 binding DNA sequences within the vicinity of the IL-17a promoter[3]. Taken together, this suggests a model where chromatin remodeling by Smarca4, possibly in interaction with Zeb1, positive regulates Th17 cells and is essential for IL-17 expression.

Conversely, among the novel 'Th17 negative' factors is Sp4, an early-induced gene, predicted in our model as a regulator of ROR-γt and as a target of ROR-γt, Batf, Irf4, Stat3 and Smarca4 (**Supplementary Fig. 13b**). Sp4 knockdown results in an increase in ROR-γt expression at 48h, and an overall stronger and "cleaner" Th17 differentiation as reflected by an increase in the expression of Th17 signature genes, including IL-17, IL-21 and Irf4, and decrease in the expression of signature genes of other CD4+ cells, including Gata3, Foxp3 and Stat4 (**Supplementary Tables 5** and **7**).

These novel and known regulatory factors act coordinately to orchestrate intra- and inter-modules interactions and to promote progressive differentiation of Th17 cells, while limiting modules that inhibit directional differentiation of this subset and promote differentiation of T cells into other T cell subsets. For instance, knockdown of Smarca4 and Zeb1 leads to decrease in Mina (due to all-positive interactions between Th17 'positive regulators'), while knockdown of Smarca4 or Mina leads to increase in Tsc22d3

expression, due to negative cross-module interactions. As we have shown using RNA-seq, these effects extend beyond the expression of regulatory factors in the network and globally affect the Th17 transcriptional program: e.g. knock-down of Mina has substantial effects on the progression of the Th17 differentiation network from the intermediate to the late phase, as some of its affected down-regulated genes significantly overlap the respective temporal clusters ($p<10^{-5}$, e.g., clusters *C9, C19*; **Supplementary Table 7**). An opposite trend is observed for the negative regulators Tsc22d3 and Sp4. For example, the transcriptional regulator Sp4 represses differentiating Th17 cells from entering into the late phase of differentiation by inhibiting the cytokine signaling (*C19*; $p<10^{-7}$) and heamatopoesis (*C20*; $p<10^{-3}$) clusters, which include Ahr, Batf, ROR-γt, etc. These findings emphasize the power of large-scale functional perturbation studies in understanding the action of complex molecular circuits that govern Th17 differentiation.

SUPPLEMENTARY METHODS

mRNA measurements on Nanostring nCounter

Details on the nCounter system are presented in full in Geiss *et al.*[4]. We used a custom CodeSet constructed to detect a total of 293 genes, selected as described above, including 18 control genes whose expression remain unaffected during the time course. Given the scarcity of input mRNA derived from each NW knockdown, a Nanostring-CodeSet specific, 14 cycle Specific Target Amplification (STA) protocol was performed according to the manufacturer's recommendations by adding 5 µL of TaqMan PreAmp Master Mix (Invitrogen) and 1 µL of pooled mixed primers (500 nM each, see **Supplementary Table 6** for primer sequences) to 5 µL of cDNA from a validated

knockdown. After amplification, 5 μL of the amplified cDNA product was melted at 95°C for 2 minutes, snap cooled on ice, and then hybridized with the CodeSet at 65°C for 16 hours. Finally, the hybridized samples were loaded into the nCounter prep station and product counts were quantified using the nCounter Digital Analyzer following the manufacturer's instructions. Samples that were too concentrated after amplification were diluted and rerun. Serial dilutions (1:1, 1:4, 1:16, & 1:64, pre-STA) of whole spleen and Th17 polarized cDNAs were used to both control for the effects of different amounts of starting input material and check for biases in sample amplification.

mRNA measurements on the Fluidigm BioMark HD

cDNA from validated knockdowns was prepared for quantification on the Fluidigm BioMark HD. Briefly, 5 μL of TaqMan PreAmp Master Mix (Invitrogen), 1 μL of pooled mixed primers (500 nM each, see **Supplementary Table 6** for primers), and 1.5 μL of water were added to 2.5 μL of knockdown validated cDNA and 14 cycles of STA were performed according to the manufacturer's recommendations. After the STA, an Exonuclease I digestion (New England Biosystems) was performed to remove unincorporated primers by adding 0.8 μL Exonuclease I, 0.4 μL Exonuclease I Reaction Buffer and 2.8 μL water to each sample, followed by vortexing, centrifuging and heating the sample to 37°C for 30 minutes. After a 15 minute 80°C heat inactivation, the amplified sample was diluted 1:5 in Buffer TE. Amplified validated knockdowns and whole spleen and Th17 serial dilution controls (1:1, 1:4, 1:16, & 1:64, pre-STA) were then analyzed using EvaGreen and 96x96 gene expression chips (Fluidigm BioMark HD)[5].

mRNA measurements using RNA-Seq

Validated single stranded cDNAs from the NW-mediated knockdowns were converted to double stranded DNA using the NEBNext mRNA Second Strand Synthesis Module (New England BioLabs) according to the manufacturer's recommendations. The samples were then cleaned using 0.9x SPRI beads (Beckman Coulter). Libraries were prepared using the Nextera XT DNA Sample Prep Kit (Illumina), quantified, pooled, and then sequenced on the HiSeq 2500 (Illumnia) to an average depth 20M reads.

Nanostring nCounter data analysis

For each sample, we divided the count values by the sum of counts that were assigned to a set of control genes that showed no change (in time or between treatments) in the microarray data (18 genes altogether). For each condition, we computed a change fold ratio, comparing to at least three different control samples treated with non-targeting (NT) siRNAs. We then pooled together the results of all pairwise comparisons (i.e. AxB pairs for A repeats of the condition and B control (NT) samples): we required a substantial fold change (above a threshold value t) in the same direction (up/ down regulation) in more than half of the pairwise comparisons. The threshold t was determined as $max\ \{d1, d2\}$, where $d1$ is the mean+std in the absolute log fold change between all pairs of matching NT samples (*i.e.*, form the same batch and the same time point; $d1$=1.66), and where $d2$ is the mean + 1.645 times the standard deviation in the absolute log fold change shown by the 18 control genes (determined separately for every

comparison by taking all the 18xAxB values; corresponding to p=0.05, under assumption of normality). We ignored all pairwise comparisons in which both NT and knockdown samples had low counts before normalization (<100).

We used a permutation test to evaluate the overlap between our predicted network model (**Fig. 2**) and the knockdown effects measured in the Nanostring nCounter (**Fig. 4, Supplementary Fig. 6**). We computed two indices for every TF for which predicted target were available: (i) specificity – the percentage of predicted targets that are affected by the respective knockdown (considering only genes measured by nCounter), and (ii) sensitivity – the percentage of genes affected by a given TF knockdown that are also its predicted targets in the model. To avoid circularity, we exclude from this analysis target genes predicted in the original network based on knockout alone. We combined the resulting values (on average, 13.5% and 24.8%, respectively) into an F-score (the harmonic mean of specificity and sensitivity). We then repeat the calculation of F-score in 500 randomized datasets, where we shuffle the target gene labels in the knockdown result matrix. The reported empirical p-value is:

P=(1+ #randomized datasets with equal of better F-score)/(1+ # randomized datasets)

Fluidigm data analysis

For each sample, we subtracted the Ct values from the geometric mean of the Ct values assigned to a set of four housekeeping genes. For each condition, we computed a fold change ratio, comparing to at least three different control samples treated with non-targeting (NT) siRNAs. We then pooled together the results of all pairwise comparisons

(i.e. AxB pairs for A repeats of the condition and B control (NT) samples): we required a substantial difference between the normalized Ct values (above a threshold value) in the same direction (up/ down regulation) in more than half of the pairwise comparisons. The threshold *t* was determined as *max {log2(1.5), d1(b), d2}*, where *d1(b)* is the mean+std in the delta between all pairs of matching NT samples (*i.e.*, from the same batch and the same time point), over all genes in expression quantile b (1<=b <=10). *d2* is the mean + 1.645 times the standard deviation in the deltas shown by 10 control genes (the 4 housekeeping genes plus 6 control genes from the Nanostring signature); *d2* is determined separately for each comparison by taking all the 10xAxB values; corresponding to p=0.05, under assumption of normality). We ignored all pairwise comparisons in which both NT and knockdown samples had low counts before normalization (Ct<21 [taking into account the amplification, this cutoff corresponds to a conventional Ct cuotff of 35]).

RNA-seq data analysis

We created a Bowtie index based on the UCSC known Gene transcriptome[6], and aligned paired-end reads directly to this index using Bowtie[7]. Next, we ran RSEM v1.11[8] with default parameters on these alignments to estimate expression levels. RSEM's gene level expression estimates (tau) were multiplied by 1,000,000 to obtain transcript per million (TPM) estimates for each gene. We used quantile normalization to further normalize the TPM values within each batch of samples. For each condition, we computed a fold change ratio, comparing to at least two different control samples treated with non-targeting (NT) siRNAs. We then pooled together the results of all pairwise comparisons (i.e. AxB pairs for A repeats of the condition and B control (NT) samples): we required a

significant difference between the TPM values in the same direction (up/ down regulation) in more than half of the pairwise comparisons. The significance cutoff *t* was determined as *max {log2(1.5), d1(b)}*, where *d1(b)* is the mean+1.645*std in the log fold ratio between all pairs of matching NT samples (*i.e.*, from the same batch and the same time point), over all genes in expression quantile b (1<=b <=20). We ignored all pairwise comparisons in which both NT and knockdown samples had low counts (TPM<10). To avoid spurious fold levels due to low expression values we add to the expression values a small constant, set to the value of the 1st quantile [out of 10] of all TPM values in the respective batch.

We use a hypergeometric test to evaluate the overlap between our predicted network model (**Fig. 2**) and the knockdown effects measured by RNA-seq (**Fig. 4d**). As background, we used all of the genes that appeared in the microarray data (and hence have the potential to be included in the network). As an additional test, we used the Wilcoxon-Mann-Whitney rank-sum test, comparing the absolute log fold-changes of genes in the annotated set to the entire set of genes (using the same background as before). The rank-sum test does not require setting a significance threshold; instead, it considers the fold change values of all the genes. The p-values produced by the rank-sum test were lower (i.e., more significant) than in the hypergeometric test, and therefore, in **Fig. 4c,** we report only the more stringent (hypergeometric) p-values.

Analysis of Tsc22d3 ChIP-seq data

ChIP-seq reads were aligned to the NCBI Build 37 (UCSC mm9) of the mouse genome

using Bowtie[9]. Enriched binding regions (peaks) were detected using MACS[10] with a p-value cutoff of 10^{-8}. We associate a peak with a gene if it falls in proximity to its 5' end (10kb upstream and 1kb downstream from transcription start site) or within the gene's body. We used the RefSeq transcript annotations for gene's coordinates.

We assess the overlap of ChIP-seq peaks with annotated genomic regions (**Supplementary Table 8**). We say that a region *A* overlap with a peak *B* if *A* is within a distance of 50bp from *B*'s summit (as determined by MACS). The regions we used include: (**i**) regulatory features annotations from the Ensemble database[11]; (**ii**) regulatory features found by the Oregano algorithm[12]; (**iii**) conserved regions annotated by the multiz30way algorithm (here we consider regions with multiz30way score>0.7); (**iv**) repeat regions annotated by RepeatMasker (http://www.repeatmasker.org); (**v**) putative promoter regions - taking 10kb upstream and 1kb downstream of transcripts annotated in RefSeq[13]; (**vi**) gene body annotations in RefSeq; (**vii**) 3' proximal regions (taking 1kb upstream and 5kb downstream to 3' end); (**viii**) regions enriched in histone marks H3K4me3 and H3K27me3 in Th17 cells [14]; (**ix**) regions enriched in binding of Stat3 and Stat5[15], Irf4 and Batf[16], and RORγt (Xiao et al unpublished) in Th17 cells, and Foxp3 in iTreg (Xiao et al., unpublished).

For each set of peaks "x" and each set of genomic regions "y", we used a binomial p-value to assess their overlap in the genome as described in [17]. The number of hits is defined as the number of x peaks that overlap with y. The background probability in sets (i)—(vii) is set to the overall length of the region (in bp) divided by the overall length of

the genome. The background probability in sets (viii)—(ix) is set to the overall length of the region divided by the overall length of *annotated* genomic regions: this includes annotated regulatory regions (as defined in sets *i*, and *ii*), regions annotated as proximal to genes (using the definitions from set *v-vii*), carry a histone mark in Th17 cells (using the definition from set *viii*), or bound by a transcription factors in Th17 cells (using the definitions from set *ix*).

For the transcription factors (set ix), we also include an additional "gene-level" test: here we evaluated the overlap between the set of bound genes using a hypergeometric p-value. We use a similar test to evaluate the overlap between the bound genes and genes that are differentially expressed in Tsc22d3 knockdown.

We repeated the analysis with a second peak-calling software (Scripture[18,19]), and obtained consistent results in all the above tests. Specifically, we saw similar levels of overlap with the Th17 factors tested, both in terms of co-occupied binding sites and in terms of common target genes.

Using literature microarray data for deriving a Th17 signature and for identifying genes responsive to Th17-related perturbations

To define the Th17 signatures genes, we downloaded and analyzed the gene expression data from Ref. [14] and preprocessed it using the RMA algorithm, followed by quantile normalization using the default parameters in the ExpressionFileCreator module of the

GenePattern suite[20]. This data includes replicate microarray measurements from Th17, Th1, Th2, iTreg, nTreg, and Naïve CD4+ T cells. For each gene, we evaluated whether it is over-expressed in Th17 cells compared to all other cell subsets using a one-sided *t*-test. We retained all cases that had a p-value < 0.05. As an additional filtering step, we required that that the expression level of a gene in Th17 cells be at least 1.25 fold higher than its expression in all other cell subsets. To avoid spurious fold levels due to low expression values, we add a small constant (c=50) to the expression values.

To define genes responsive to published Th17-related perturbations, we downloaded and analyzed gene expression data from several sources that provided transcriptional profiles of Th17 cells under various conditions (listed above). These datasets were preprocessed as above. To find genes that were differentially expressed in a given condition (compared to their respective control), we computed the fold change between the expression levels of each probeset in the case and control conditions. To avoid spurious fold levels due to low expression values, we add to the expression values a small constant as above. We only reported cases where more than 50% of all of the possible case-control comparisons were above a cutoff of 1.5 fold change. As an additional filter, when duplicates are available, we computed a Z-score as above and only reported cases with a corresponding p-value < 0.05.

SUPPLEMENTARY FIGURES AND LEGENDS

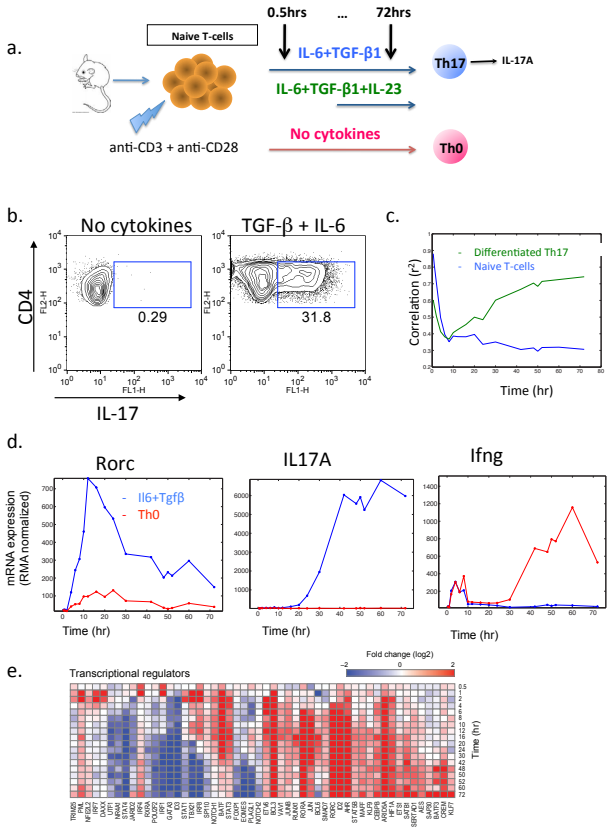

Supplementary Figure 1. Treatment of Naïve CD4+ T-cells with TGF-β1 and IL-6 for three days induces the differentiation of Th17 cells. (**a**) Overview of the time course experiments. Naïve T cells were isolated from WT mice, and treated with IL-6 and TGF-β1. We then used microarrays to measure global mRNA levels at 18 different time points (0.5hr-72hr, **Methods**). As a control, we used the same WT naïve T cells under Th0 conditions harvested at the same 18 time points. For the last four time points (48hr - 72hr), we also profiled cells treated with IL-6, TGF-β1, and IL-23. (**b**) Generation of Th17 cells by IL-6 and TGF-β1 polarizing conditions. FACS analysis of naïve T cells

differentiated with TGF-β1 and IL-6 (right) shows enrichment for IL-17 producing Th17 T cells; these cells are not observed in the Th0 controls. (**c**) Comparison of the obtained microarray profiles to published data from naïve T-cells and differentiated Th17 cells (Wei et. al, 2009; Supplemental Ref. 9). Shown is the Pearson correlation coefficient (Y axis) between each of our 18 profiles (ordered by time point, X axis) and either the naïve T cell profiles (blue) or the differentiated Th17 profiles (green). Our expression profiles gradually transition from a naïve-like state (at t=0.5hr, $r^2>0.8$, $p<10^{-10}$) to a Th17 differentiated state (at t=72hr, $r^2>0.65$, $p<10^{-10}$). (**d**) Expression of key cytokines. Shown are the mRNA levels (Y axis) as measured at each of the 18 time points (X axis) in the Th17 polarizing (blue) and Th0 control (red) conditions for the key Th17 genes RORc (left) and IL-17a (middle), both induced, and for the cytokine IFN-γ, unchanged in our time course. **(e)** Transcriptional profiles of key transcriptional regulators. Shown are the differential expression levels (log2(ratio)) for each gene (column) at each of 18 time points (rows) in Th17 polarizing conditions (TGF-β1 and IL-6; left panel, Z-normalized per row) vs. control activated Th0 cells.

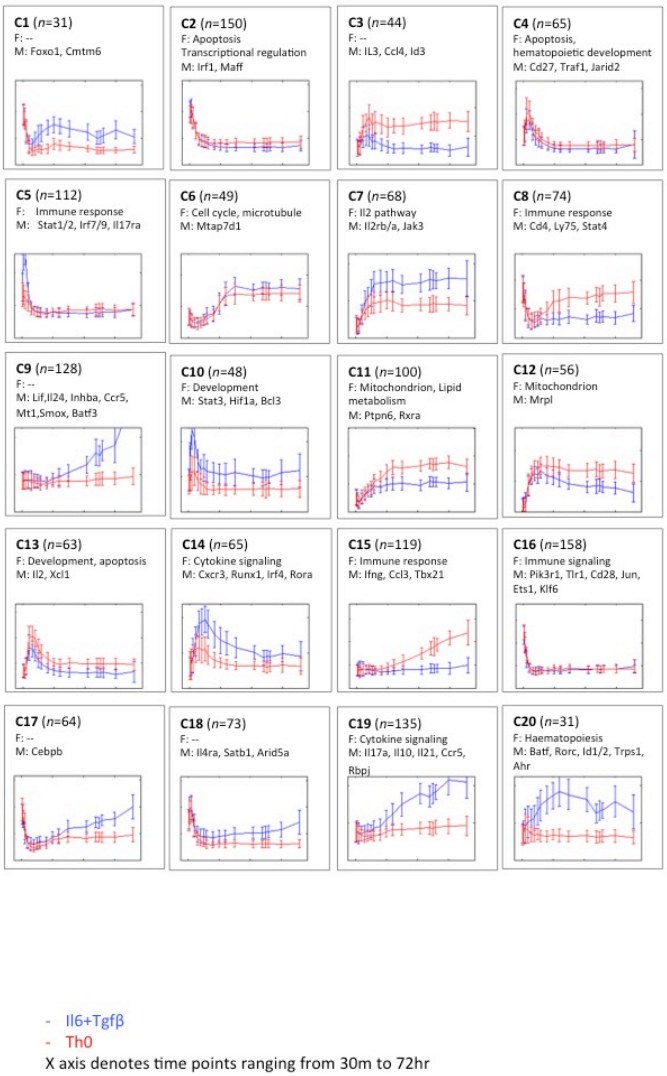

Supplementary Figure 2. Clusters of differentially expressed genes in the Th17 time course data. For each of the 20 clusters in **Fig. 1b** shown are the average expression levels (Y axis, ± standard deviation, error bars) at each time point (X axis) under Th17 polarizing (blue) and Th0 (red) conditions. The cluster size ("n"), enriched functional annotations ("F"), and representative member genes ("M") are denoted on top.

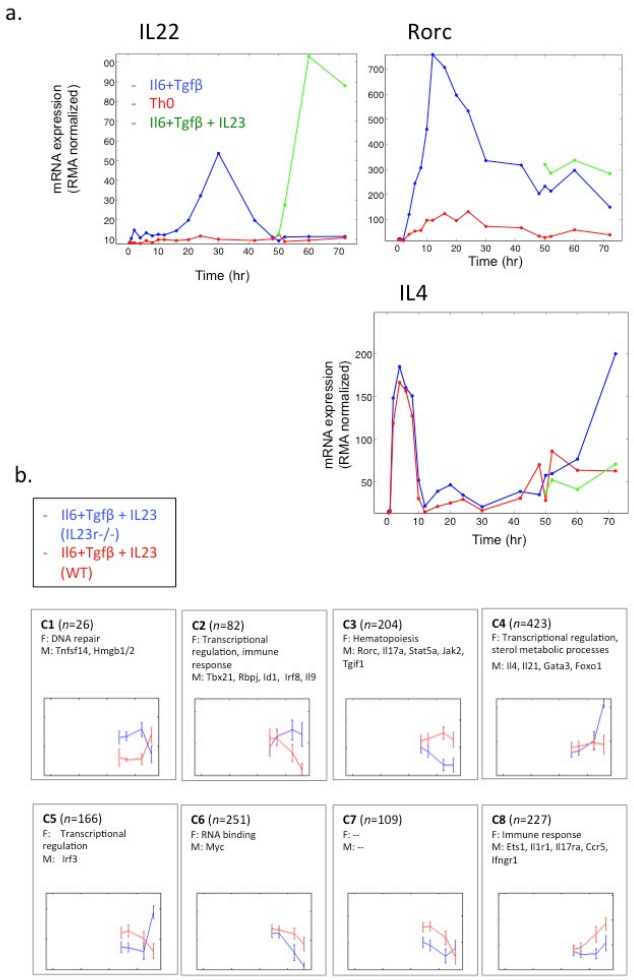

Supplementary Figure 3. Transcriptional effects of IL-23.

The late phase response depends in part on IL-23, as observed when comparing temporal transcriptional profiles between cells stimulated with TGF-β1+IL-6 versus TGF-β1+IL-6+IL-23, or between WT and IL-23r$^{-/-}$ cells treated with TGF-β1+IL-6+IL-23. For instance, in IL-23r-deficient Th17 cells, the expression of IL-17ra, IL-1r1, IL-21r, ROR-γt, and Hif1a is decreased, and IL-4 expression is increased. The up-regulated genes in the IL-23r$^{-/-}$ cells are enriched for other CD4+ T cell subsets, suggesting that, in the absence of IL-23 signaling, the cells start to de-differentiate, thus further supporting the

hypothesis that IL-23 may have a role in stabilizing the phenotype of differentiating Th17 cells (see also **Supplementary Table 1**).

Shown are: (**a**) Transcriptional profiles of key genes. Shown are the expression levels (Y axis) of three key genes (IL-22, RORc, IL-4) at each time point (X axis) in Th17 polarizing conditions (blue), Th0 controls (red), and following the addition of IL-23 (beginning at 48hr post differentiation) to the Th17 polarizing conditions (green). (**b**) IL-23-dependnet transcriptional clusters. Shown are clusters of differentially expressed genes in the IL-23r$^{-/-}$ time course data (blue) compared to WT cells, both treated with Th17 polarizing cytokines and IL23 (red). For each cluster, shown are the average expression levels (Y axis, ± standard deviation, error bars) at each time point (X axis) in the knockout (blue) and wildtype (red) cells. The cluster size ("n"), enriched functional annotations ("F"), and representative member genes ("M") are denoted on top.

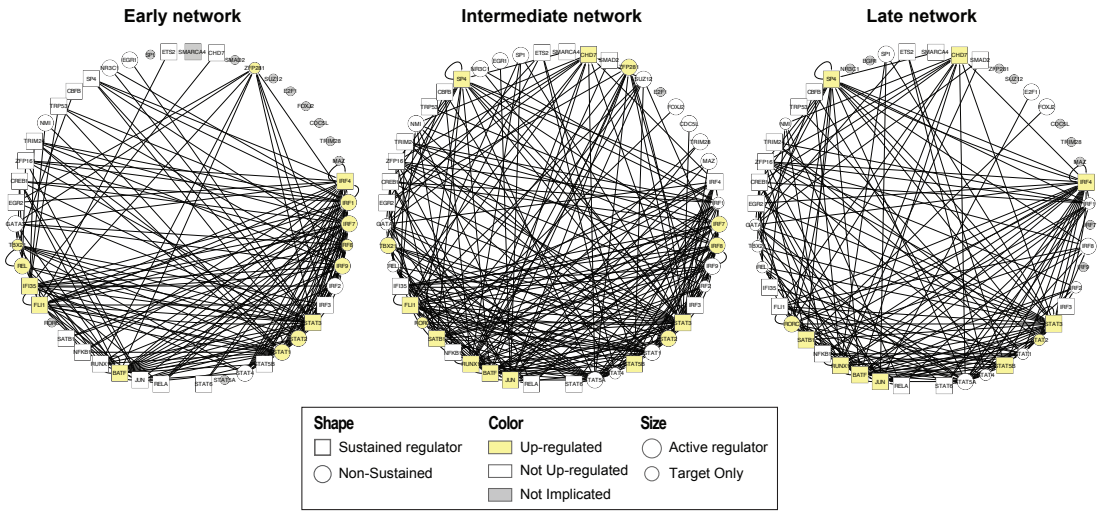

Supplementary Figure 4. At the heart of each network is its 'transcriptional circuit', connecting active TFs to target genes that themselves encode TFs. The transcription factor circuits shown (in each of the 3 canonical networks) are the portions of each of the inferred networks (**Supplementary Table 3)** associating transcription factors to targets that themselves encode transcription factors. Yellow nodes denote transcription factor genes that are over-expressed (compared to Th0) during the respective time segment. Edge color reflects the data type supporting the regulatory interaction (legend).

The transcriptional circuit in the early-response network connects 48 factors that are predicted to act as regulators to 72 factors whose own transcript is up- or down-regulated during the first four hours (a subset of this model is shown in the **left panel**; see **Supplementary Table 3** for the complete model). The circuit automatically highlights many TFs that were previously implicated in immune signaling and Th17 differentiation, either as positive or negative regulators, including Stat family members, both negative (Stat1, Stat5) and positive (Stat3), the pioneering factor Batf, TFs targeted by TGF-β

signaling (Smad2, Runx1, and Irf7), several TFs targeted by TCR signaling (Rel, Nfkb1, and Jun), and several interferon regulatory factors (Irf4 and Irf1), positioned both as regulators and as target genes that are strongly induced. In addition, 34 regulators that were not previously described to have a role in Th17 differentiation were identified (*e.g.*, Sp4, Egr2, and Smarca4). Overall, the circuit is densely intraconnected, with 16 of the 48 regulators themselves transcriptionally controlled (*e.g.*, Stat1, Irf1, Irf4, Batf). This suggests feedback circuitry, some of which may be auto-regulatory (*e.g.*, for Irf4, Stat3 and Stat1). As in the early network, there is substantial cross-regulation between the 64 TFs in the intermediate and late transcriptional circuits (**middle** and **right panels** respectively), which include major Th17 regulators such as ROR-γt, Irf4, Batf, Stat3, and Hif1a (see **Supplementary Table 3** for the complete models).

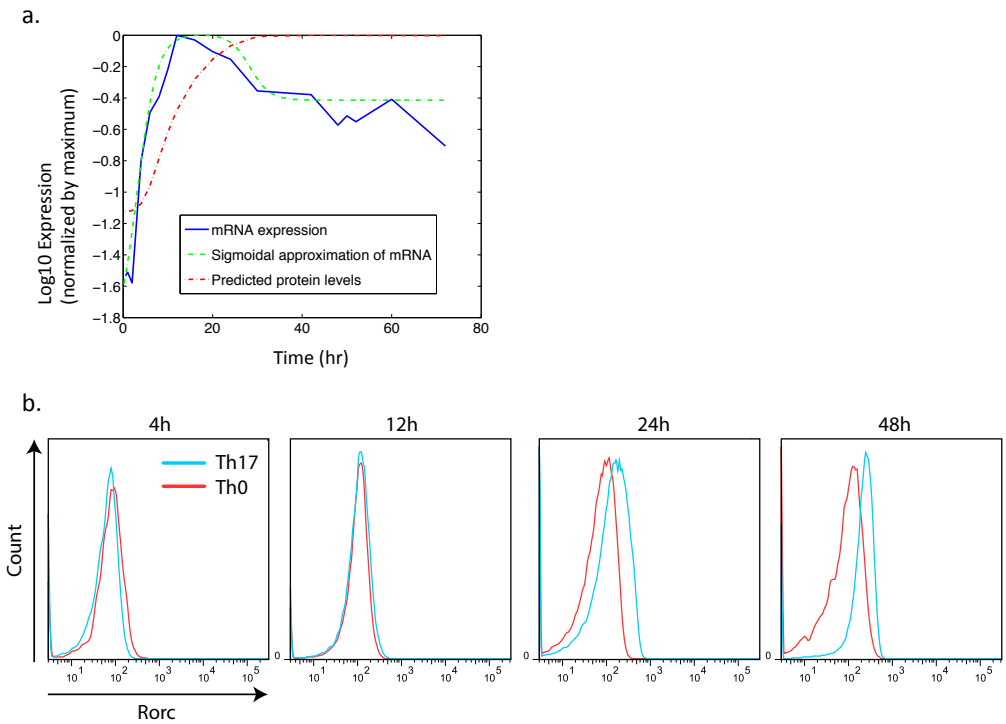

Supplementary Figure 5. Predicted and validated protein levels of ROR-γt during Th17 differentiation. (**a**) Shown are RORγt mRNA levels along the original time course under Th17 polarizing conditions, as measured with microarrays (blue). A sigmoidal fit for the mRNA levels (green) is used as an input for a model (based on Ref. [21]) that predicts the level of RORγt protein at each time point (red). **(b)** Distribution of measured ROR-γt protein levels (x axis) as determined by FACS analysis in Th17 polarizing conditions (blue) and Th0 conditions (red) at 4, 12, 24, and 48hr post stimulation.

a.

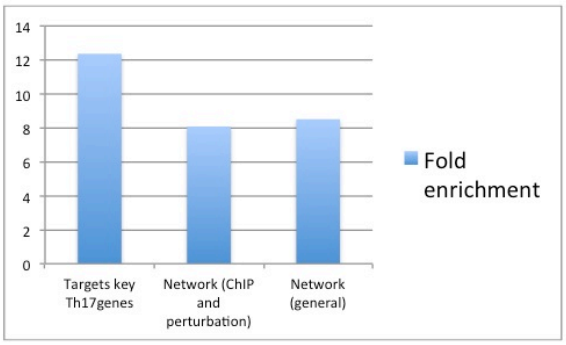

b.

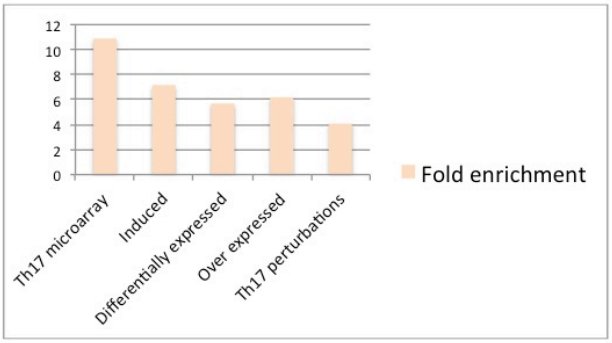

Supplementary Figure 6. Predictive features for ranking candidates for knockdown. Shown is the fold enrichment (Y axis, in all cases, $p<10^{-3}$, hypergeometric test) in a curated list of known Th17 factors for different (a) network-based features and (b) expression-base features (as used in **Fig. 3a**).

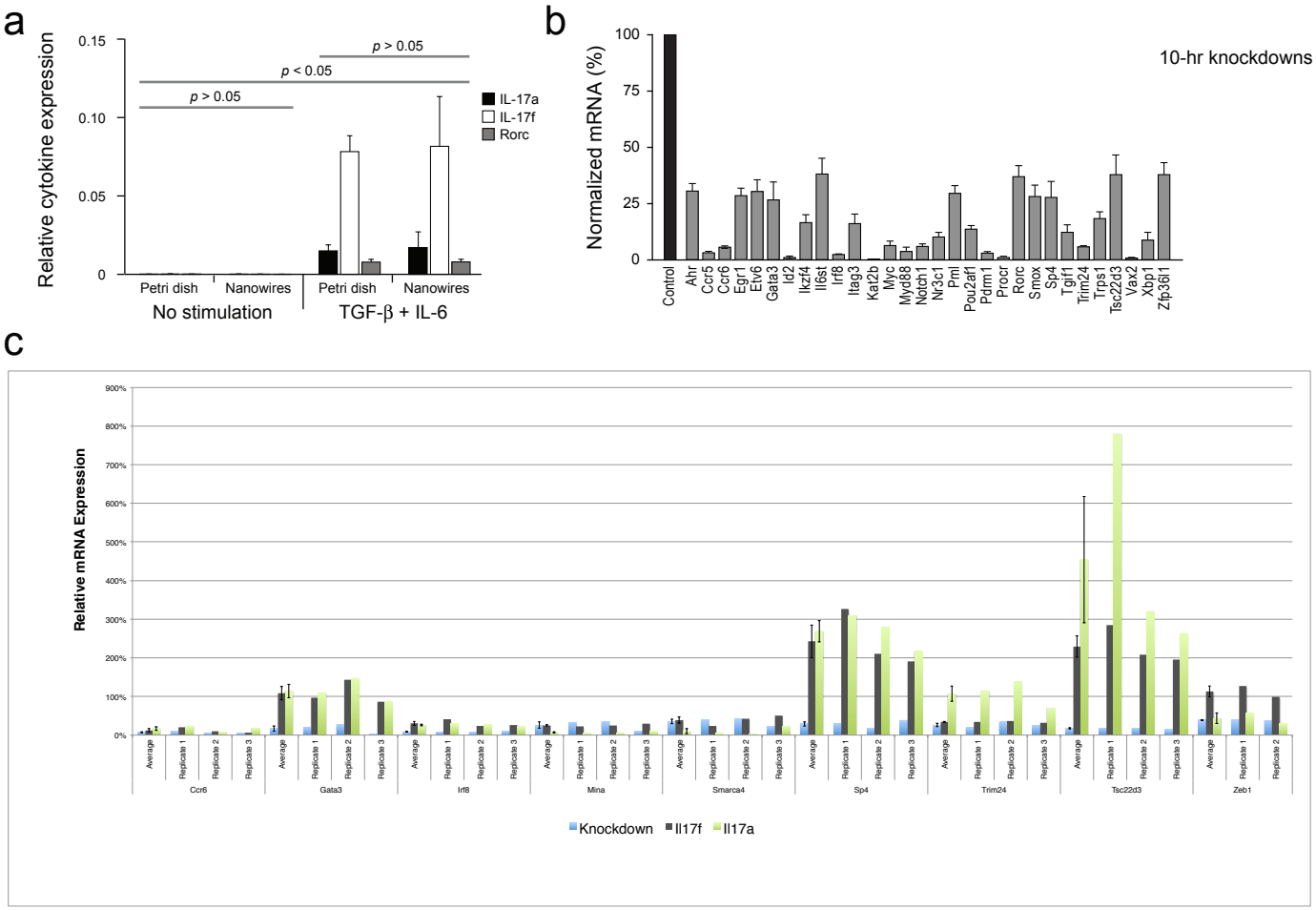

Supplementary Figure 7. Nanowire activation on T-cells, knockdown at 10h, and consistency of NW-based knockdowns and resulting phenotypes. (**a**) Nanowires do not activate T cells and do not interfere with physiological stimuli. Shown are the levels of mRNA (mean ± standard error, n = 3) for key genes, measured 48hr after activation by qPCR (Y axis, mean and standard error of the mean), in T cells grown in petri dishes (left) or on silicon nanowires (right) without polarizing cytokines ('no cytokines') or in the presence of Th17 polarizing cytokines ('TGF-β1 + IL6'). (**b**) Effective knockdown by siRNA delivered on nanowires. Shown is the % of mRNA remaining after knockdown (by qPCR, Y axis: mean ± standard error relative to non-targeting siRNA control, n = 12, black bar on left) at 10 hours after introduction of polarizing cytokines. The genes presented are a superset of the 39 genes selected for transcriptional profiling.

(c) Shown are average target transcript reductions and phenotypic changes (as measured by IL-17f and IL-17a expression) for three different experiments of NW-based knockdown (from at least 2 different cultures) of 9 genes at 48 hours post stimulation. Light blue bars: knockdown level (%remaining relative to siRNA controls); dark grey and light green bars: mRNAs of IL-17f and IL-17a, respectively, relative to siRNA controls.

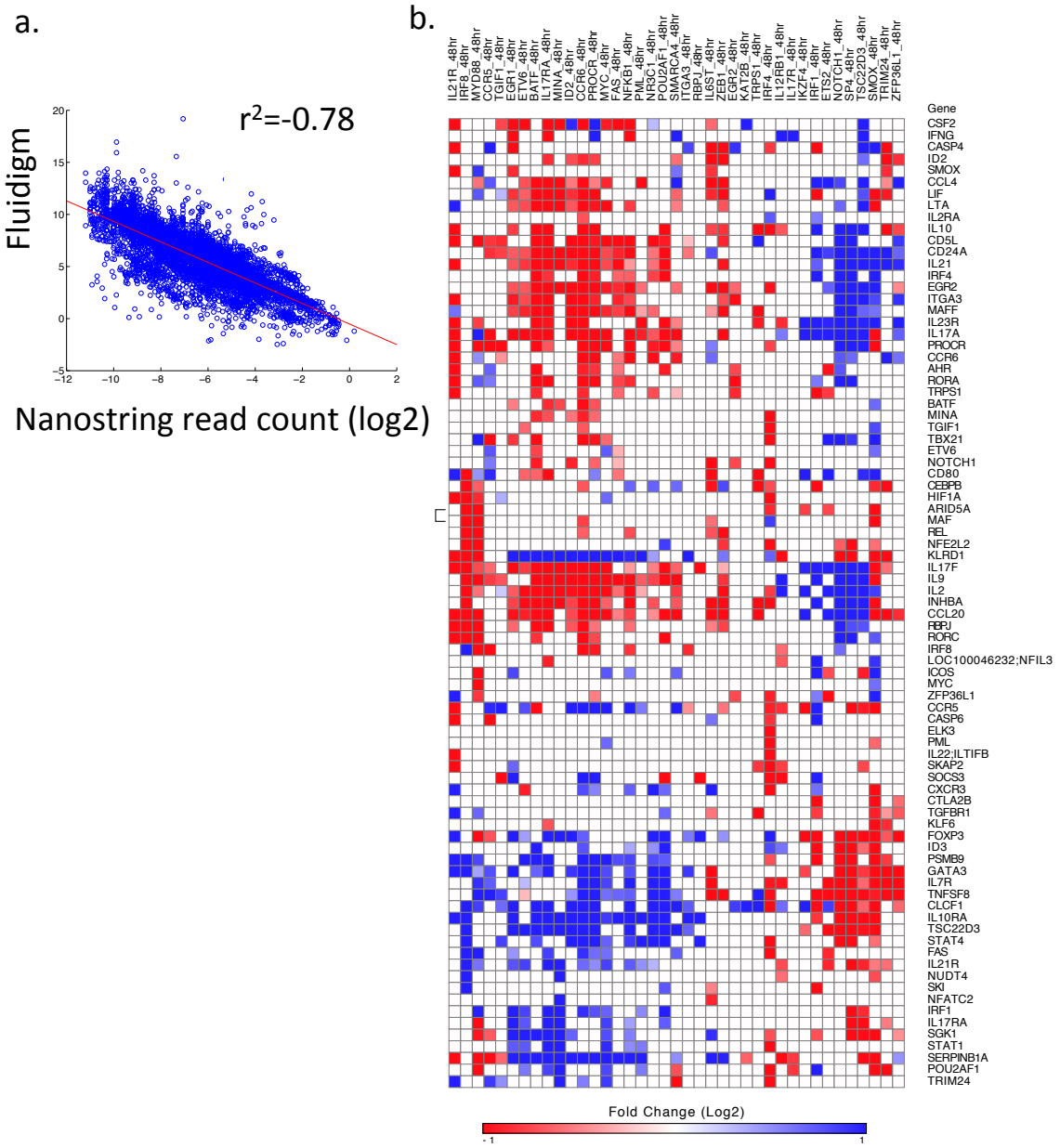

Supplementary Figure 8. Cross-validation of the Nanostring expression profiles for each nanowire-delivered knockdown using Fluidigm 96x96 gene expression chips. (**a**) Comparison of expression levels measured by Fluidigm (Y axis) and Nanostring (X axis) for the same gene under the same perturbation. Expression values were normalized to control genes as described in **Methods**. (**b**) Analysis of Fluidigm data recapitulates the partitioning of targeted factors into two modules of positive and negative Th17

regulators. Shown are the changes in transcription of the 86 gene signature (rows) following knockdown of each factor (columns).

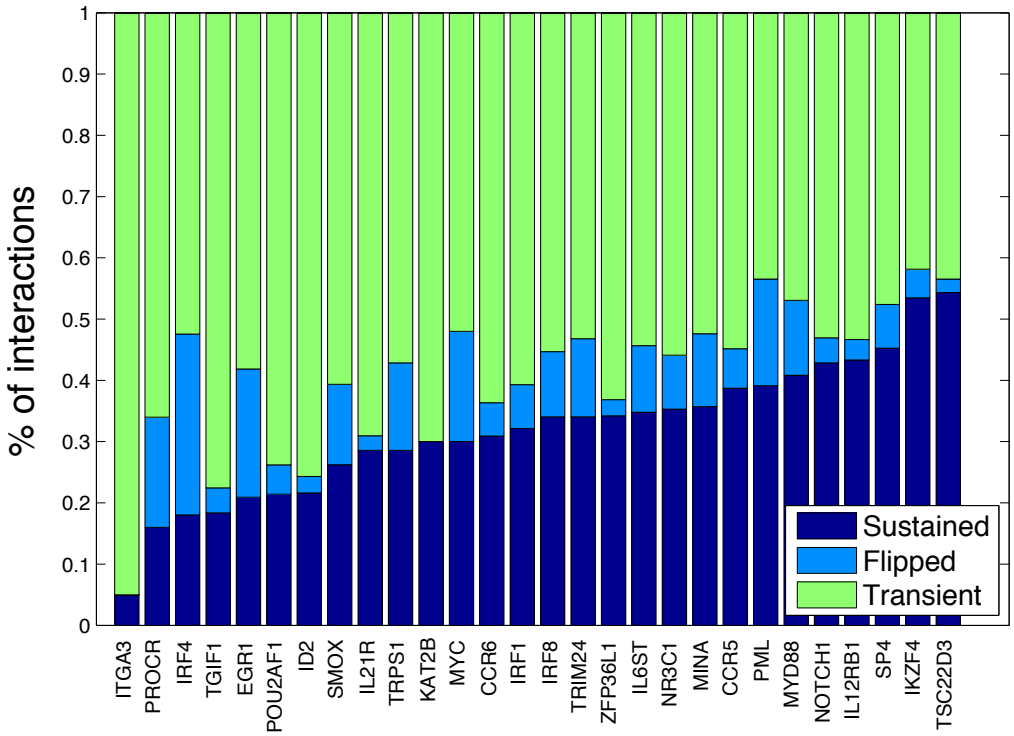

Supplementary Figure 9. Rewiring of the Th17 "functional" network between 10hr to 48hr post stimulation. For each regulator that was profiled at 10hr and 48hr, we calculate the percentage of "edges" (i.e., gene *A* is affected by perturbation of gene *B*) that either appear in the two time points with the same activation/repression logic (Sustained); appear only in one time point (Transient); or appear in both networks but with a different activation/repression logic (Flipped). In the sustained edges, the perturbation effect (fold change) has to be significant in at least one of the time point (Methods), and consistent (in terms of activation/repression) in the other time point (using a more permissive cutoff of 1.25 fold).

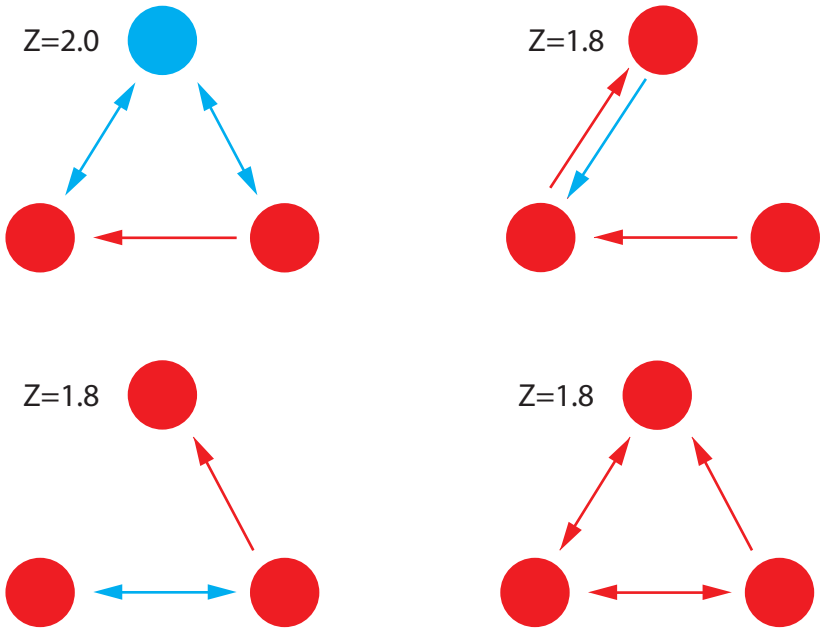

Supplementary Figure 10. "Chromatic" network motifs. We used a 'chromatic' network motif analysis to find recurring sub networks with the same topology and the same node and edge colors. Shown are the four significantly enriched motifs ($p<0.05$). Red nodes: positive regulators; blue nodes: negative regulator; red edges from A to B: knockdown of A downregulates B; blue edge: knockdown of A upregulates B. Motifs were found using the FANMOD software [22].

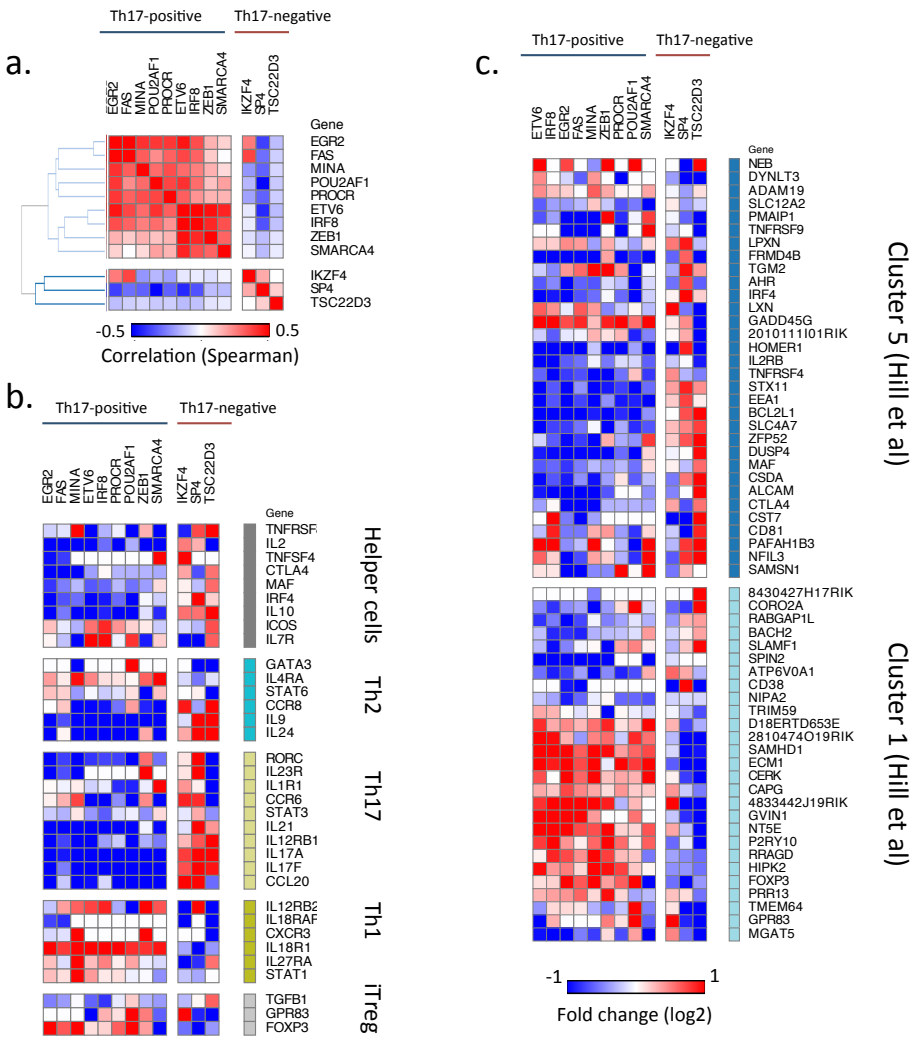

Supplementary Figure 11. RNA-seq analysis of nanowire-delivered knockdowns

(**a**) Correlation matrix of knockdown profiles. Shown is the Spearman rank correlation coefficient between the RNA-Seq profiles (fold change relative to NT siRNA controls) of regulators perturbed by knockdowns. Genes that were not significantly differentially expressed in any of the samples were excluded from the profiles. (**b**) Knockdown effects on known marker genes of different CD4+ T cell lineages. Shown are the expression levels for canonical genes (rows) of different T cell lineages (labeled on right) following knockdown of each of 12 regulators (columns). Red/Blue: increase/decrease in gene

expression in knockdown compared to non-targeting control (**Methods**). Shown are only genes that are significantly differentially expressed in at least one knockdown condition. The experiments are hierarchically clustered, forming distinct clusters for Th17-positive regulators (left) and Th17-neagtive regulators (right). **(c)** Knockdown effects on two sub-clusters of the T-regulatory cell signature, as defined by Hill et al[23]. Each cluster (annotated in Hill et al as Clusters 1 and 5) includes genes that are over expressed in T-regs cells compared to conventional T cells. However, genes in Cluster 1 are more correlated to Foxp3 and responsive to Foxp3 transduction. Conversely, genes in cluster 1 are more directly responsive to TCR and IL-2 and less responsive to Foxp3 in Treg cells. Knockdown of Th17-positive regulators strongly induces the expression of genes in the 'Foxp3' Cluster 1. The knockdown profiles are hierarchically clustered, forming distinct clusters for Th17-positive regulators (left) and Th17-neagtive regulators (right). Red/Blue: increase/decrease in gene expression in knockdown compared to non-targeting control (**Methods**). Shown are only genes that are significantly differentially expressed in at least one knockdown condition.

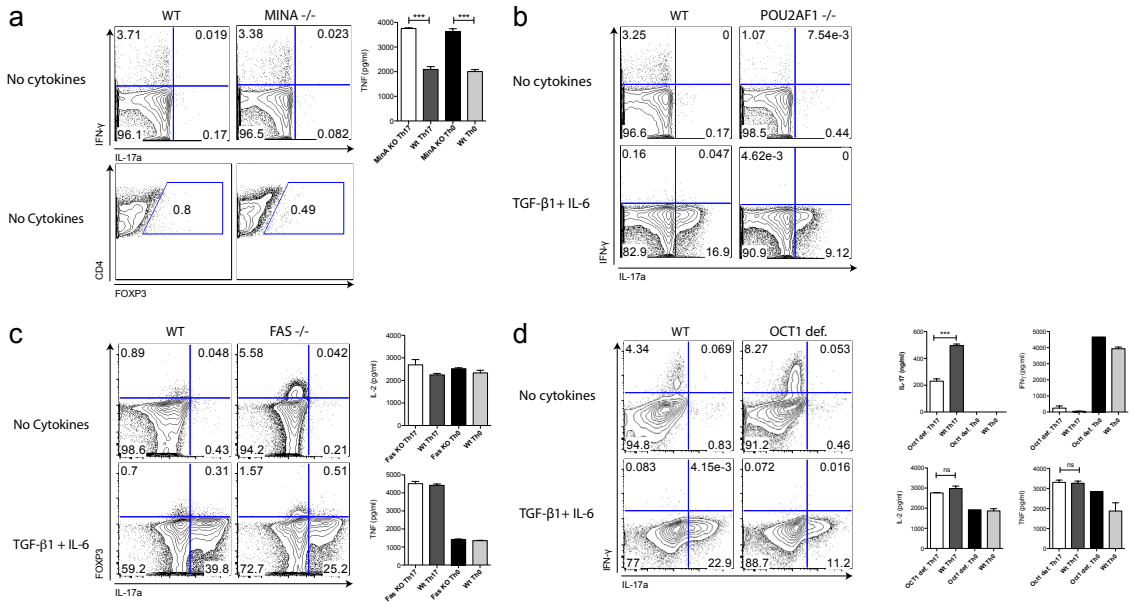

Supplementary Figure 12. Quantification of cytokine production in knockout cells at 72h of in-vitro differentiation using Flow cytometry and Enzyme-linked immunosorbent assay (ELISA).

All flow cytometry figures shown, except for Oct1, are representative of at least 3 repeats, and all ELISA data has at least 3 replicates. For Oct1, only a limited amount of cells were available from reconstituted mice, allowing for only 2 repeats of the Oct1 deficient mouse for flow cytometry and ELISA. **(a, left)** Mina$^{-/-}$ T cells activated under Th0 controls are controls for the graphs shown in **Fig. 5a**. **(a, right)** TNF secretion by Mina$^{-/-}$ and WT cells, as measured by cytometric bead assay showing that Mina-/- T cells produce more TNF when compared to control. **(b)** Intracellular cytokine staining of Pou2af1$^{-/-}$ and WT cells for IFN-γ and IL-17a as measured by flowcytometry. **(c, left)** Flow cytometric analysis of Fas$^{-/-}$ and WT cells for Foxp3 and Il-17 expression. **(c, right)** IL-2 and Tnf secretion by Fas$^{-/-}$ and WT cells, as measured by a cytokine bead assay ELISA. **(d, left).** Flow cytometry on Oct1$^{-/-}$ and WT cells for IFN-γ and IL-17a,

showing an increase in IFN-γ positive cells in the Th0 condition for the Oct1 deficient mouse. **(d, right**) Il-17a, IFN-γ, IL-2 and TNF production by Oct1$^{-/-}$ and WT cells, as measured by cytokine ELISA and cytometric bead assay. Statistical significance in the ELISA figures is denoted by: * $p < 0.05$, ** $p < 0.01$, and *** $p < 0.001$.

a. b.

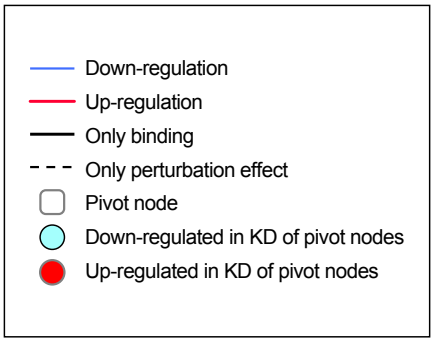

Supplementary Figure 13. Zeb1, Smarca4, and Sp4 are key novel regulators affecting the Th17 differentiation programs. Shown are regulatory network models centered on different pivotal regulators (square nodes): (a) Zeb1 and Smarca4, and (b) Sp4. In each network, shown are the targets and regulators (round nodes) connected to the pivotal nodes based on perturbation (red and blue dashed edges), TF binding (black solid edges), or both (red and blue solid edges). Genes affected by perturbing the pivotal nodes are colored (red: target is up-regulated by knockdown of pivotal node; blue: target is down-regulated).

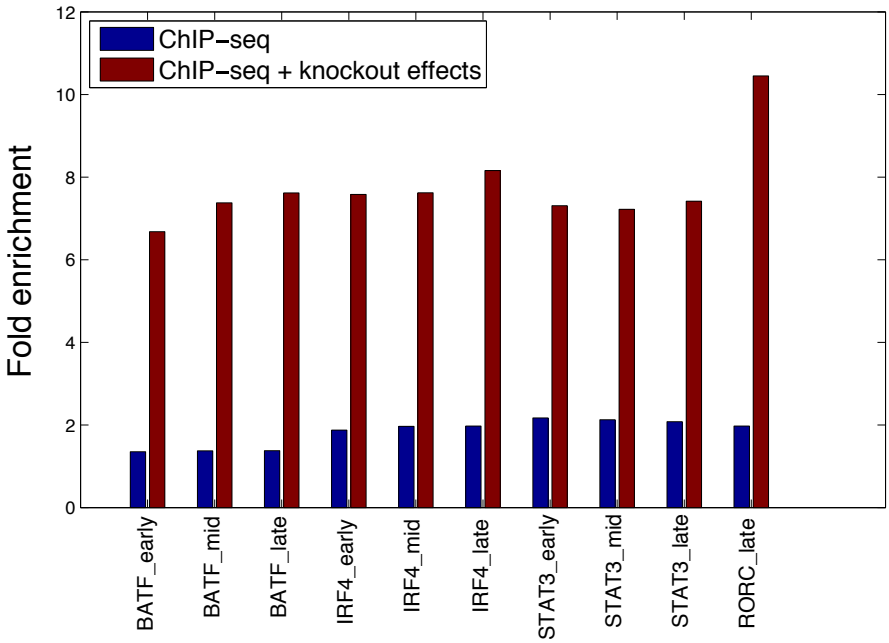

Supplementary Figure 14. Overlap with ChIP-seq and RNA-seq data from Ciofani et al (Cell, 2012). Fold enrichment is shown for the four TF that were studied by Ciofani et al using ChIP-seq and RNA-seq and are predicted as regulators in our three network models (early, intermediate [denoted as "mid"], and late). We compare to the ChIP-seq based network of Ciofani et al. (blue) and to their combined ChIP-seq/RNA-seq network (taking a score cutoff of 1.5, as described by the authors; red). In all cases the p-value of the overlap (with ChIP-seq only or with the combined ChIP-seq/ RNA-seq network) is below 10^{-10} (using Fisher exact test), but the fold enrichment is particularly high in genes that are both bound by a factor and affected by its knockout, the most functional edges.

Supplementary Table Legends

Supplementary Table 1. List of microarray probesets that were differentially expressed in the TGF-β1+Il6 microarray data. Columns: DE score and DE score IL-23r$^{-/-}$ vs. WT: number of differential expression methods that identify a particular probe in the original experiment and the experiment with IL-23r$^{-/-}$ cells, respectively; Columns Cluster and IL-23r$^{-/-}$ cluster ID: cluster assignment in each experiment (**Fig. 1b**, **Supplementary Fig. 2** and **3)**; Columns {TF or chromatin modifier, Cell surface, Cytokine activity, In Codeset}: 1 indicates inclusion, 0 exclusion.

Supplementary Table 2. Functional enrichments for expression clusters. Tabs present enrichments for: (1) clusters for the combined Th0 and Th17 microarray data, (2) genes up or down-regulated in the Th17 microarray data relative to Th0, (3) genes up or down regulated in time, (4) genes differentially expressed upon the addition of IL-23, and (5) genes differentially expressed in IL-23r$^{-/-}$ cells relative to their WT counterparts.

Supplementary Table 3. **Regulatory interactions in the three canonical temporal networks (Early, Intermediate, and Late).** For each of the three consecutive networks, listed are the TFs active in the network, their regulatory targets, supporting evidence and its source for regulatory interactions, p-value (defined by the statistical significance of the overlap between the putative targets of the TF [according to the respective data source] and the gene group to which the target gene belongs), and the time stamp of regulation (**Methods**).

Supplementary Table 4. Table of ranked regulators of Th17 differentiation. Sheet 1: Presented is a ranked list of the regulators (**Methods**), including those displayed in **Fig. 3a**. For columns {Knocked down, Attempted knockdown, Known, Th17 microarray signature, Targets key molecules, ChIP and phenotype (IPA), Predicted Regulator, Induced, Is overexpressed in Th17 time course}: 1 denotes inclusion, 0 exclusion; for columns {DE score in Th17 time course, DE score in IL23-/-}: number of methods (out of 4 used for the Th17 time course and 3 for the IL23-/- data) by which the gene was reported as differentially expressed. Column 'Expression changes in key perturbations in Th17 cells': the number of corroborating pieces of evidence, 1- between 2 to 3 sources; 2 – more than 3 sources; 0 –otherwise (**Methods**). The "Comments" column presents rationale for selecting low-ranking genes that were successfully knocked down. **Sheet 2:** a similar ranked list for receptor genes.

Supplementary Table 5. Results of Nanostring nCounter and Fluidigm analysis. Sheet 1: List of signature genes (including control genes); **Sheets 2-3**: Expression fold changes (log2) at the 10hr (Fluidigm) and 48hr (Nanostring) time points. Presented are only fold changes above the inference cutoff (**Methods**).

Supplementary Table 6. Primers for Nanostring STA and qRT-PCR/Fluidigm and siRNA sequences. Sheet 1: Presented are the sequences for each forward and reverse primer used in the Fluidigm/qRT-PCR experiments and Nanostring nCounter gene expression profiling. **Sheet 2**: Sequences for RNAi used for knockdown analysis.

Supplementary Table 7. RNA-seq data analysis.

Sheet 1: Differentially expressed genes. Values shown are $\log_2$ of fold change (compared to a non-targeting siRNA control). Displayed are all genes with a significant fold change in at least one condition; comparisons that did not pass our differential expression criteria are marked as "0". **Sheet 2**: Overlap with gene signatures. For each annotated set of genes (e.g., a temporal cluster from our data), we test for its enrichment with genes differentially expressed following knockdown. We test for the significance of the enrichment using two different tests (and hence present two p-values): (i) a hypergeometric test, evaluating the overlap between the differentially expressed genes and the genes in the cluster; (**ii**) A Wilcoxon-Mann-Whitney rank-sum test, comparing the absolute fold-change values of genes in the annotated set to the entire set of genes; **Sheet 3**: TF binding enrichment analysis of differentially expressed genes. We used a hypergeometric p-value to evaluate the overlap between sets of differentially expressed genes and sets of bound genes as determined by ChIP-seq. The ChIP-Seq data is from Th17 cells unless indicated otherwise on the second column.

Supplementary Table 8. Tsc22d3 ChIP-seq data analysis.

Sheet 1: overlaps with annotated regions. Two types of analysis are presented: (i) a genomic-region based score – evaluating the overlap between the sites bound by Tsc22d3 (as determined using MACS[10]) and annotated genomic regions. We used a binomial p-value[17] to assess the significance of the overlap. (ii) a gene-based analysis, evaluating the overlap between the set of genes that are proximal to sites bound by Tsc22d3 and the

indicated sets of genes, using a hypergeometric p-value. **Sheet 2:** overlaps– list of all the Tsc22d3 binding regions and their overlaps with annotated genomic regions.

Supplementary References

1 Sánchez-Tilló, E. *et al.* ZEB1 represses E-cadherin and induces an EMT by recruiting the SWI/SNF chromatin-remodeling protein BRG1. *Oncogene* **29**, 3490-3500, doi:10.1038/onc.2010.102 (2010).

2 Zhang, F. & Boothby, M. T helper type 1-specific Brg1 recruitment and remodeling of nucleosomes positioned at the IFN-gamma promoter are Stat4 dependent. *J. Exp. Med.* **203**, 1493-1505, doi:10.1084/jem.20060066 (2006).

3 Matys, V. *et al.* TRANSFAC: transcriptional regulation, from patterns to profiles. *Nucleic Acids Res.* **31**, 374-378 (2003).

4 Geiss, G. K. *et al.* Direct multiplexed measurement of gene expression with color-coded probe pairs. SI. *Nature Biotechnology* **26**, 317-325, doi:10.1038/nbt1385 (2008).

5 Dalerba, P. *et al.* Single-cell dissection of transcriptional heterogeneity in human colon tumors. *Nat Biotechnol* **29**, 1120-1127, doi:10.1038/nbt.2038 (2011).

6 Fujita, P. A. *et al.* The UCSC Genome Browser database: update 2011. *Nucleic Acids Res.* **39**, D876-882, doi:10.1093/nar/gkq963 (2011).

7 Langmead, B., Trapnell, C., Pop, M. & Salzberg, S. L. Ultrafast and memory-efficient alignment of short DNA sequences to the human genome. *Genome Biol* **10**, R25, doi:10.1186/gb-2009-10-3-r25 (2009).

8 Li, B. & Dewey, C. N. RSEM: accurate transcript quantification from RNA-Seq data with or without a reference genome. *BMC Bioinformatics* **12**, 323, doi:10.1186/1471-2105-12-323 (2011).

9 Langmead, B., Trapnell, C., Pop, M. & Salzberg, S. L. in *Genome Biol* Vol. 10 R25 (2009).

10 Zhang, Y. *et al.* in *Genome Biol* Vol. 9 R137 (2008).

11 Flicek, P. *et al.* Ensembl 2011. *Nucleic Acids Res.* **39**, D800-806, doi:10.1093/nar/gkq1064 (2011).

12 Smith, R. L. *et al.* Polymorphisms in the IL-12beta and IL-23R genes are associated with psoriasis of early onset in a UK cohort. *J Invest Dermatol* **128**, 1325-1327, doi:5701140 [pii]

10.1038/sj.jid.5701140 (2008).

13 Pruitt, K. D., Tatusova, T. & Maglott, D. R. NCBI reference sequences (RefSeq): a curated non-redundant sequence database of genomes, transcripts and proteins. *Nucleic Acids Res.* **35**, D61-65, doi:10.1093/nar/gkl842 (2007).

14 Wei, G. *et al.* in *Immunity* Vol. 30 155-167 (2009).

15 Yang, X. P. *et al.* Opposing regulation of the locus encoding IL-17 through direct, reciprocal actions of STAT3 and STAT5. *Nat. Immunol.* **12**, 247-254, doi:10.1038/ni.1995 (2011).

16 Glasmacher, E. *et al.* A Genomic Regulatory Element That Directs Assembly and Function of Immune-Specific AP-1-IRF Complexes. *Science*, doi:10.1126/science.1228309 (2012).

17 Mclean, C. Y. *et al.* in *Nature biotechnology* Vol. 28 nbt.1630-1639 (2010).

18 Guttman, M. *et al.* in *Nature biotechnology* Vol. 28 503-510 (2010).

19 Garber, M. *et al.* A High-Throughput Chromatin Immunoprecipitation Approach Reveals Principles of Dynamic Gene Regulation in Mammals. *Molecular cell*, doi:10.1016/j.molcel.2012.07.030 (2012).

20 Reich, M. *et al.* GenePattern 2.0. *Nat. Genet.* **38**, 500-501, doi:10.1038/ng0506-500 (2006).

21 Schwanhäusser, B. *et al.* Global quantification of mammalian gene expression control. *Nature* **473**, 337-342, doi:10.1038/nature10098 (2011).

22 Wernicke, S. & Rasche, F. FANMOD: a tool for fast network motif detection. *Bioinformatics (Oxford, England)* **22**, 1152-1153, doi:10.1093/bioinformatics/btl038 (2006).

23 Hill, J. A. *et al.* Foxp3 transcription-factor-dependent and -independent regulation of the regulatory T cell transcriptional signature. *Immunity* **27**, 786-800, doi:S1074-7613(07)00492-X [pii]
10.1016/j.immuni.2007.09.010 (2007).